Development of Omnidirectional Optical Terminals for Swarm Communications and Navigation

Jose E. Velazco,* Alexa C. Aguilar,* Andy R. Klaib,* Uriel S. Escobar,* Sean E. Cornish,* Joseph C. Griffin*

ABSTRACT. — JPL is developing a new omnidirectional optical terminal that will provide fast communications and accurate navigation for swarms of spacecraft. The omnidirectional optical communicator/navigator (OOCN) under development presents a truncated icosahedral geometry that contains arrays of miniature laser telescopes and optical detectors. The miniature optical telescopes are located at the center of each OOCN facet and allow for full sky coverage. The optical detectors, symmetrically deployed on each vertex of the OOCN body, have two purposes: to receive fast incoming communications signals and accurately determine the angle of arrival (AOA) of the incoming signal. The continuous AOA tracking performed by the OOCN mechanism makes it ideally suited for swarm navigation as well. In this paper, we provide a general description of the main OOCN features: 1) high data rate communications, 2) full sky coverage, and 3) ability to maintain multiple links simultaneously. The current OOCN prototype operates at a wavelength of 650 nm, and uses low-power single-mode laser diodes and fast silicon photodetectors. We present the latest experimental results of AOA and pointing testing obtained with this prototype in our optical laboratory. Lastly, we present examples of future missions that could be enabled by the OOCN.

I. Introduction

Small spacecraft, such as CubeSats and small satellites (SmallSats), are affordable, relatively easy to deploy, and can allow the rapid demonstration of new space technologies. When compared to their larger flagship counterparts, small spacecraft have the potential to provide outstanding science returns at possibly a small fraction of the cost. In addition, small spacecraft are key in enabling new technologies, such as swarms, interconnected spacecraft with the potential to operate autonomously, share data, and act as a large "synthetic" sensor.

Swarms furnished with high-resolution sensors will demand more bandwidth while requiring lower size, weight, and power (SWaP), resulting in a need for low-power, low-

* Communications Ground Systems Section.

The research described in this publication was carried out by the Jet Propulsion Laboratory, California Institute of Technology, under a contract with the National Aeronautics and Space Administration.

SWaP optical transceivers capable of multigigabit link rates. Optical transceivers have the potential to provide order-of-magnitude improvements over existing radio frequency (RF) transceivers [1–4]. This technology is already widespread in the telecommunications industry in the form of fiber-optic links, but free-space optical communication has yet to be explored in full depth. The interspacecraft omnidirectional optical communicator/navigator (OOCN) currently under development at JPL for applications in swarms and constellations promises gigabit per second data rates, full sky coverage, and multiple link capability (see Figure 1) [5, 6]. The OOCN will provide adaptable high data rate communications as well as highly accurate swarm metrology.

In this article, we provide a general overview of the OOCN development. Section II provides a description of the OOCN. Section III presents the main features of this technology. Section IV shows the latest results obtained with the OOCN prototype whereas Section V illustrates potential future missions enabled by the OOCN. Final conclusions are presented in Section VI.

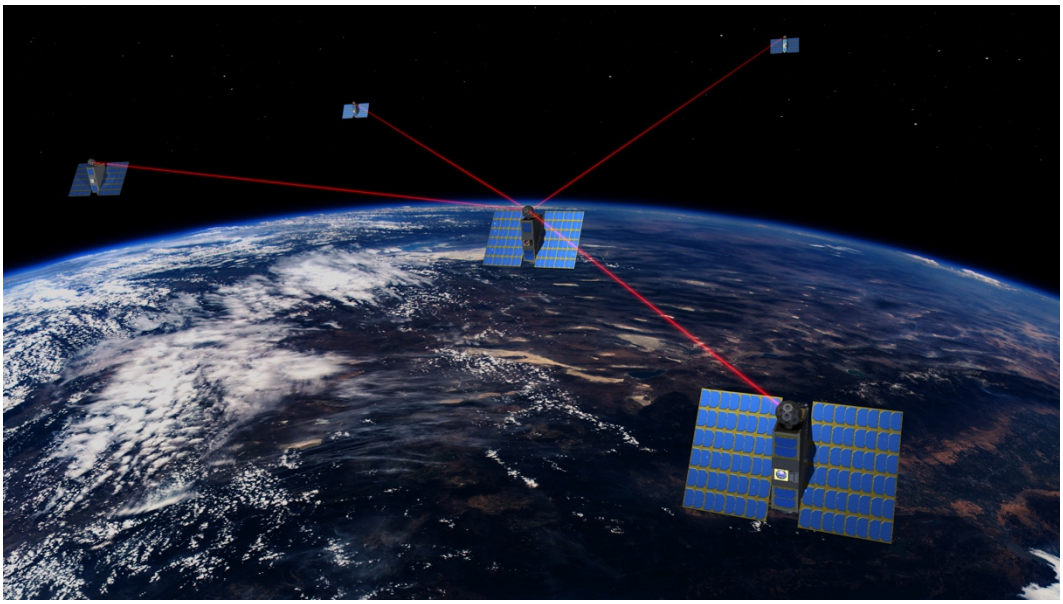

Figure 1. Swarm of SmallSats enabled by the Interspacecraft Optical Communicator/Navigator.

II. Description

The OOCN employs arrays of laser telescopes and detectors fitted inside a truncated icosahedron geometry to provide full sky coverage (see Figure 2). Each telescope provides fine beam steering within its field of regard via a compact micro electro mechanical system (MEMS) mirror [7]. The photodetectors are strategically arranged around the OOCN body and used for continuous angle-of-arrival (AOA) calculation of the incoming signals. The detectors are also used to process the communications information contained on the optical beam. The OOCN provides full sky coverage (4π steradians) and maintains multiple gigabit links simultaneously. The OOCN has the potential to provide high data rate communications not only for interspacecraft cross-links but for ground uplinks and downlinks as well.

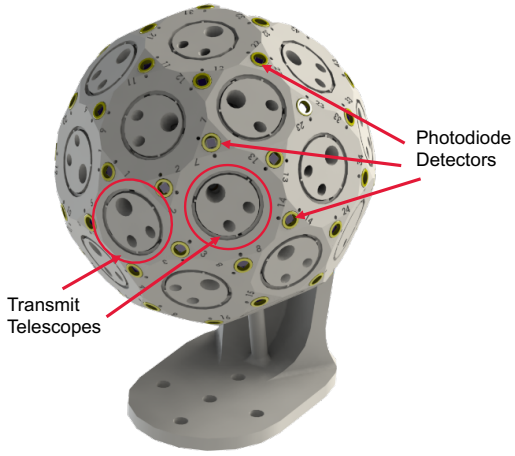

Figure 2. OOCN truncated icosahedron geometry.

The OOCN was designed with the goal of enabling fast and continued connectivity for swarms and constellations of spacecraft. A basic block diagram of the OOCN is shown in Figure 3. The arrays of lasers telescopes and detectors fitted inside the icosahedron body are connected to a fast field-programmable-gate-array (FPGA) processor. The FPGA reads the information from the detectors and provides commands to actuate the MEMS mirrors, and sends the communications signals that modulate the laser diodes.

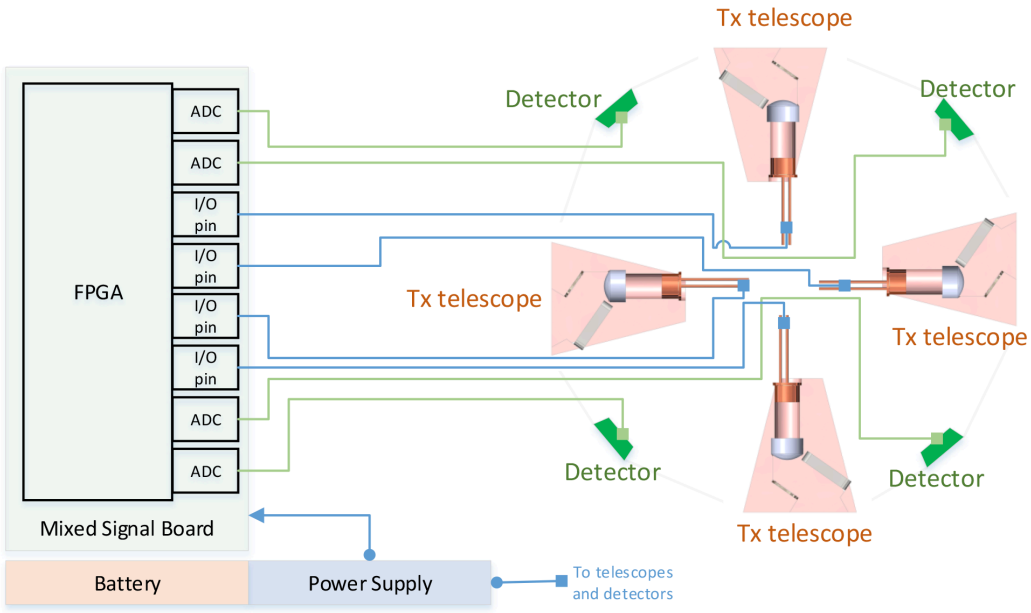

Figure 3. Simplified block diagram of the OOCN.

A. Transmit Telescopes

The OOCN transmit telescopes are conically shaped and include a laser diode, a collimator, a mirror, a MEMS steering mirror [7], and a biconcave lens (Figure 4). The telescope geometry is optimized for beam transport efficiency (minimize beam clipping) along the various optical components. The telescope is also miniaturized to allow the insertion of multiple telescopes around the OOCN body.

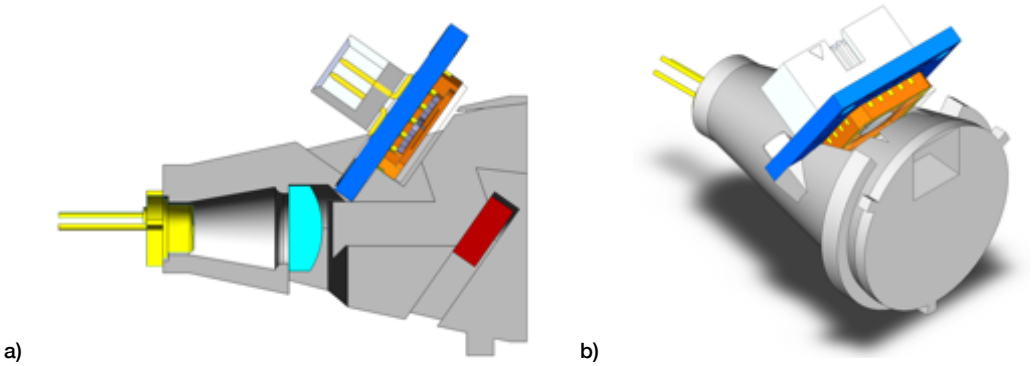

a) b)

Figure 4. Images of the OOCN telescopes (biconcave lens not shown).

The beam produced by the laser diode, after collimation, is reflected toward the MEMS mirror via the fixed mirror. The MEMS mirror has the ability to steer the beam at fast velocities. The biconcave lens extends beam steering by a factor of ~2. Optical beam steering provided by this OOCN telescope design is ±22°.

B. Receive Photodetectors

The photodetectors are strategically arranged around the OOCN body for continuous AOA calculation of incoming signals using suitable AOA algorithms. The photodetectors are also fast enough to receive the high data rate optical communications signals. We are currently exploring two options, silicon PIN photodetectors and avalanche photodetectors (APDs) (Figure 5) .

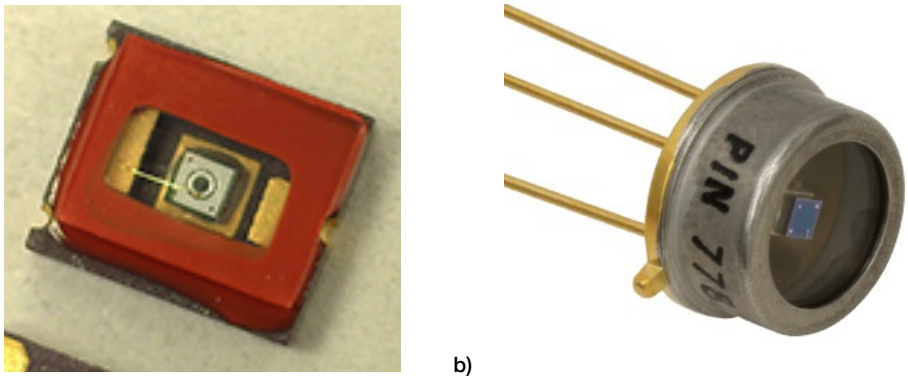

a) b)

Figure 5. Images of a) avalanche and b) PIN photodetectors mounted on suitable headers.

PIN detectors feature larger active areas and require low operating voltages. Their junction capacitance is ~5 pF, which yields a rise time of 1 ns. APDs use larger voltages that allow reducing their capacitance, and hence depict faster rise times than their PIN counterparts. Also, due to the avalanche effect, APDs feature high gains, which substantially increase their responsivity.

C. Pointing and Tracking

As mentioned earlier, the OOCN employs arrays of miniature transmit (Tx) telescopes and receive (Rx) photodetectors to provide secure high data rate communications. The Tx

telescopes receive pointing commands and communications data from an FPGA whereas the Rx photodetectors feed the incoming signals to the FPGA via suitable analog-to-digital converters (ADCs). The Tx telescopes are used to transmit the communications signals to neighboring OOCNs. The Rx photodiodes receive optical communications signals from other spacecraft and allow the bearing and elevation of the incoming signals to be determined via a proprietary technique. Once bearing and elevation of the incoming signal is calculated by the FPGA, the OOCN can direct the appropriate telescope to communicate with the generator of the incoming signal.

III. OOCN Capabilities

In this section, we describe the main capabilities of the current OOCN embodiment (shown in Figure 2). The main features of the OOCN are: a) fast data rates, b) full sky (4π steradian) coverage, and c) ability to maintain multiple links simultaneously.

A. Fast Data Rates

In order to achieve fast connectivity, the OOCN transceivers include fast modulatable laser diodes and avalanche photodetectors. A schematic of the transmitter and receiver system is shown in Figure 6. The photodetector receives the incoming light and converts it to a low current signal. A transimpedance amplifier (TIA) takes in the low current signal and translates it to a measurable voltage. This voltage is used for analyzing the content of the incoming signal. We measure the amplitude and temporal variations of the incoming signal.

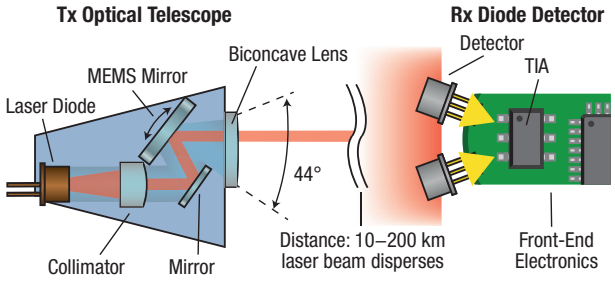

Figure 6. Schematic of the OOCN Tx optical telescope and Rx photodiode detectors.

For our application, we sought to optimize the design of the OOCN transceiver to allow fast communications at the distances of interest. One key parameter that we optimized is receiver sensitivity, with the goal of obtaining a receiver that could detect very low power optical signals.

In general, the sensitivity of the receiver shown in Figure 6, in dBm, is given by,

$$S_{Rx} = 10 \cdot \log\left[i_n \cdot \frac{SNR}{\Re \cdot G} \cdot \frac{1}{2}\left(\frac{r_e - 1}{r_e + 1} \right) \cdot 10^3 \right],$$

where i_n is the input-referred noise current of the TIA, $\Re$ is the responsivity of the photodetector, G is the detector gain, SNR is the signal to noise ratio, and r_e is the extinguishing ratio of the signal. (Here we assume on-off keying modulation of the optical

beam.) For example, for $\Re = 0.5$ A/W, $i_n = 55 \cdot 10^9$ A, $G = 100$, $r_e = 10$, $SNR = 11.2$, we obtain a receiver sensitivity of $S_{Rx} = -51$ dBm.

B. Full Sky Coverage

The OOCN will provide coverage of the entire 4π steradian sky. For a truncated icosahedral geometry, each of the 32 facets should provide a coverage of at least 0.4 steradian.

1. Pointing

For transmission, the OOCN uses a set of telescopes — one telescope per facet. The telescopes use a MEMS mirror that provides 22° optical steering and a biconcave lens that enhances beam steering by a factor of ~2 to 44°. The optical steering per telescope is ~0.6 steradian, which allows for overlapping coverage among neighboring telescopes and thus, full sky coverage. Each telescope receives both steering commands and communications signals from the FPGA. A small MEMS driver board is used to interface a MEMS mirror with the FPGA. The FPGA sends serial commands to the printed circuit board (PCB), which in turn produces the appropriate voltages to steer the mirror. In Figure 7, we show the coverage provided by the various OOCN neighboring telescopes. Note that each telescope provides a coverage of 0.6 steradian using its own MEMS mirror and that no blinds spots exist.

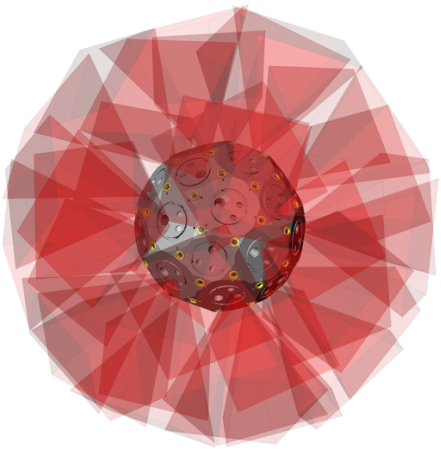

Figure 7. Image showing coverage of OOCN transmit telescopes. Note that the small overlap in coverage between neighboring telescopes ensures full sky coverage.

2. Angle of Arrival

A key component of the OOCN is its AOA system, which consists of an array of detectors placed at each vertex of the OOCN body (Figure 8) and a microcontroller. The detectors are placed on the vertices of the OOCN's truncated icosahedral frame and therefore cover every possible AOA of the incoming signals. It should be noted that for the ranges of interest, the optical beam arriving to an OOCN would be several meters in diameter. This means that when an optical beam strikes the OOCN, half of the detectors will be illuminated.

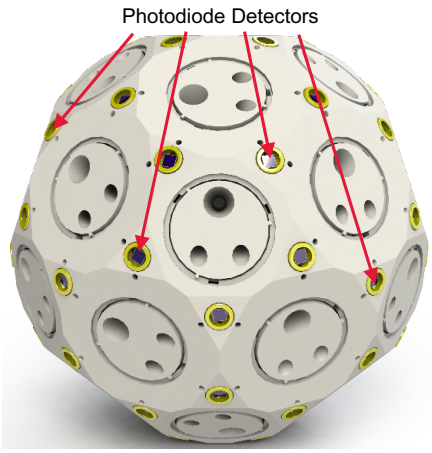

Figure 8. Schematic of the OOCN showing the location of the photodetectors (golden rings) that allow full sky coverage.

When multiple spacecraft need to communicate with an OOCN, protocols such as time-division-multiple-access (TDMA) would need to be implemented so that AOA could be correctly calculated. We also plan to use a multiple access protocol (such as TDMA) to ensure high data rate communications among multiple spacecraft.

3. Swarm Navigation

SmallSat missions have the potential of delivering substantial science return, at a portion of the cost of larger flagship counterparts. Further, if SmallSats can be configured in clusters or swarms, the technological and science return could equal or eventually surpass the returns of larger ships. Two key technical challenges for realizing spacecraft swarms are: 1) fast and stable interconnectivity among the spacecraft, and 2) adequate metrology to accurately and continuously determine the exact position of the ships forming the swarm.

Swarm Metrology. The OOCN is a key enabling technology for future swarms. The optical beams generated by the OOCN, in addition to fast interspacecraft communications, allow for continuous swarm metrology. That is to say, the OOCN allows the spacecraft forming a swarm to continuously measure azimuth and elevation of the neighboring spacecraft. Intersatellite distance could be obtained by performing additional signal processing such as a pulse-based time of flight (ToF) measurement [8]. Consequently, during typical swarm operation, the mothership has continuous knowledge of the position, (r, ϕ, θ), of each spacecraft forming the swarm (Figure 9).

We also envision that all spacecraft forming the swarm could be furnished with chip-sized rubidium clocks such as the Microsemi Space Chip-Scale Atomic Clock (CSAC) [9]. These clocks should provide coherent timing for several minutes. Since all clocks will inevitably deviate from the true time, a periodic synchronization method would be required to minimize relative timing differences within the swarm.

Swarm Synthetic Aperture. A key feature of spacecraft swarms is their ability to form a large synthetic aperture. Under this arraying arrangement, the mothership, having knowledge of the exact position of each daughtership, could send commanding information to the

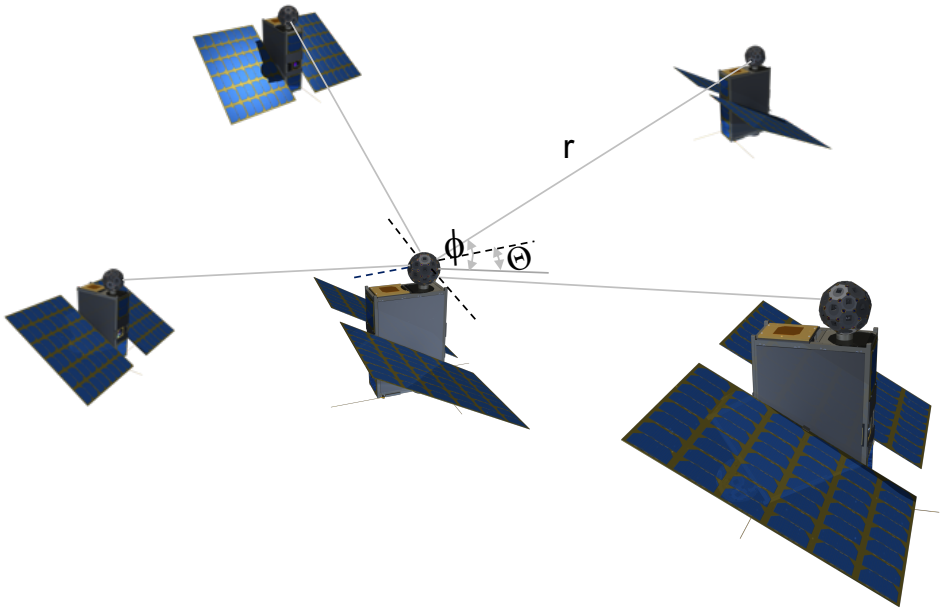

Figure 9. The OOCN will allow for continuous metrology (calculation of (r, φ, Θ)) among spacecraft forming a swarm.

daughterships that controls the phase of each ship's transmit pulse. The total swarm transmit power would be equal to the sum of each SmallSat's transmit power. Conversely, on receive, the mothership could send the same synchronizing commands, so that appropriate phase shifts are applied to each spacecraft, before combining the receiving pulses.

IV. Prototype Testing

Over the duration of this project, we have built several prototypes of the OOCN. Figure 10 shows a recent OOCN prototype during testing in our optical laboratory.

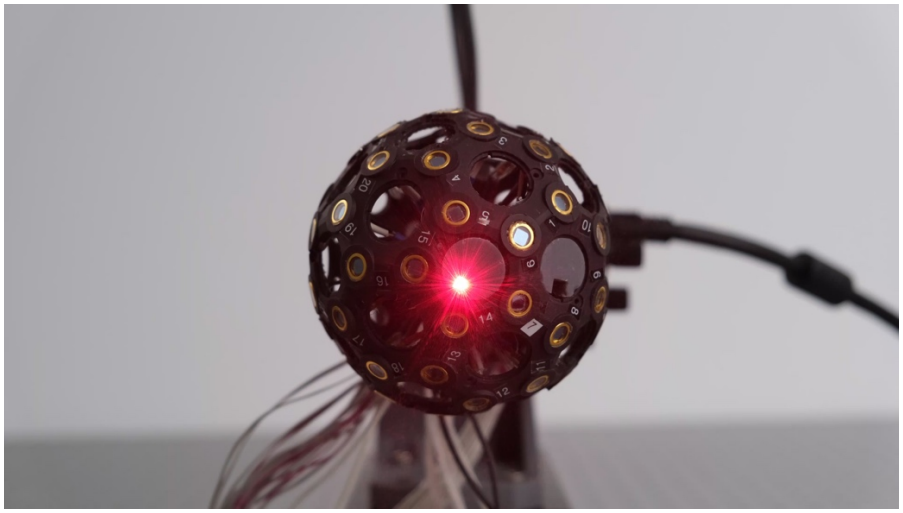

Figure 10. Picture of a recent OOCN prototype during testing in our optical laboratory.

A. AOA Testing

For angle-of-arrival testing, we employed the apparatus shown in Figure 11. The OOCN under testing is installed on a computer-controlled pan-tilt unit (PTU) platform. The PTU platform is programmed to move in azimuth and elevation (with millidegree accuracy) to emulate motion between two spacecraft. The fast photodiode detectors are connected to the microcontroller via suitable analog to digital convertors. A ~6-inch diameter, uniform-density 650 nm beam is used to illuminate the entire OOCN body. When illuminated by a uniform optical beam, the microcontroller reads the values of all detectors and calculates azimuth and elevation of the incoming signal using our AOA technique. A Python-based graphic user interface running on a laptop is used to extract AOA information from the microcontroller via a serial connection for postprocessing and real-time displaying. An image of the OOCN AOA display is shown in Figure 12. The dots displayed on the interface depict the location of all detectors and telescopes. This 3-D interface shows in real time the detectors being illuminated by the laser (dots change color from gray to blue when illuminated), the AOA calculation, and the selected telescope chosen for closing the link (the telescope dot changes color to magenta). As the OOCN is rotated with respect to the laser (via the PTU), only the detectors illuminated by the laser light up. The interface also shows the telescope (as a blue dot) that could be used to close the link at that time.

Once the OOCN is installed as shown in Figure 11, using our graphic interface (Figure 12), we verify that the OOCN is responding properly as we command various PTU positions. Subsequently, we proceed to perform AOA accuracy and precision testing whereby we gradually rotate the PTU and begin logging data.

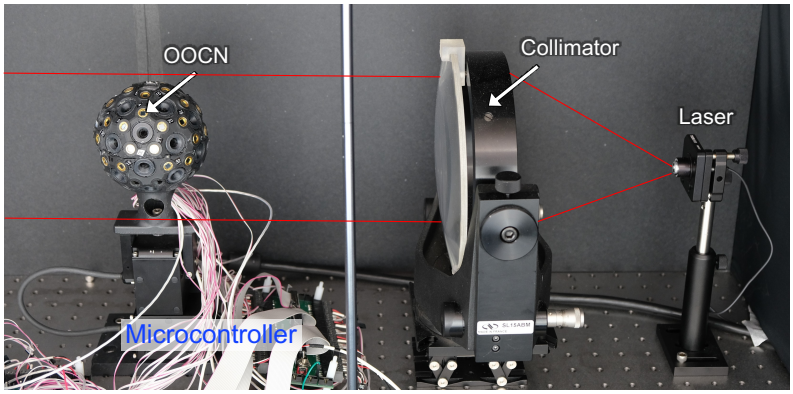

Figure 11. Setup used for testing angle of arrival.

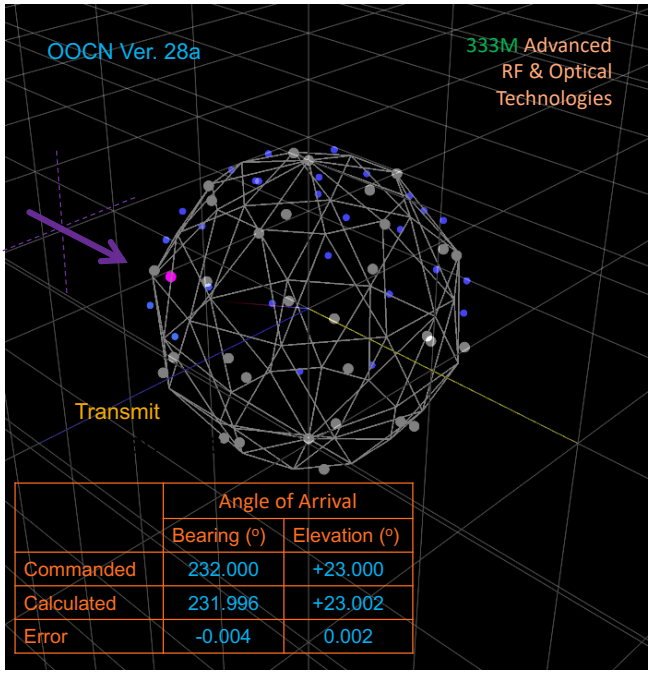

Figure 12. Python interface used to monitor AOA testing of the OOCN in real time. The blue dots indicate the detectors that are illuminated by the laser beam. The magenta dot shows the chosen telescope (based on the calculated AOA) for closing the link.

Figure 13 shows a plot of the measured AOA as a function of PTU position. The PTU position is the command sent to the PTU unit (measured via the PTU's encoder). Every time we send a position command to the PTU, we measure the encoder and calculate AOA using our algorithm. The main focus of this test was measuring AOA precision, where we take a large amount of data points as we rotate the PTU unit and determine the repeatability of the measurement. The orange squares represent measurements at each PTU position. Note the high degree of precision obtained during these tests. For the purposes of measuring error, we use root mean square (RMS) calculations. The RMS precision error obtained so far is ~76 millidegrees.

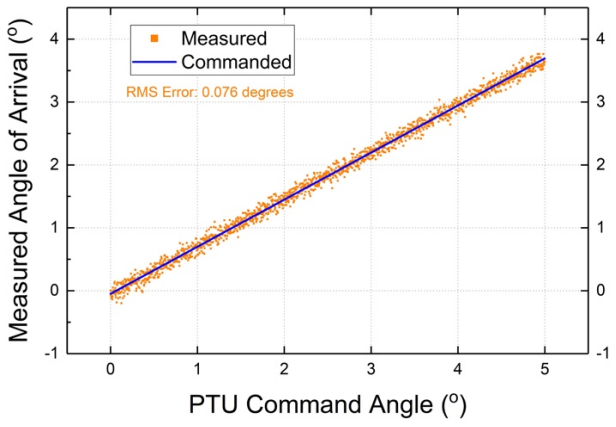

Figure 13. Plot of measured AOA as a function of PTU commanded angle. This plot shows the AOA precision obtained so far (0.076° RMS).

We are pursuing several steps to improve our AOA test setup, which include refining alignment of the OOCN with respect to the PTU unit as well as verifying proper positioning of the detectors on the OOCN body. Our goal is to achieve AOA accuracy and precision with RMS errors of a few millidegrees. Future AOA accuracy measurements using the upgraded experimental apparatus will be presented in follow-on reports.

B. Beam Pointing Testing

As part of our prototype development, we have also performed beam steering testing using the OOCN MEMS mirror. The setup used for this testing includes a MEMS mirror located inside a telescope and a large area position-sensing device (PSD) (see Figure 14). The PSD measures optical beam displacement with micron-level resolution.

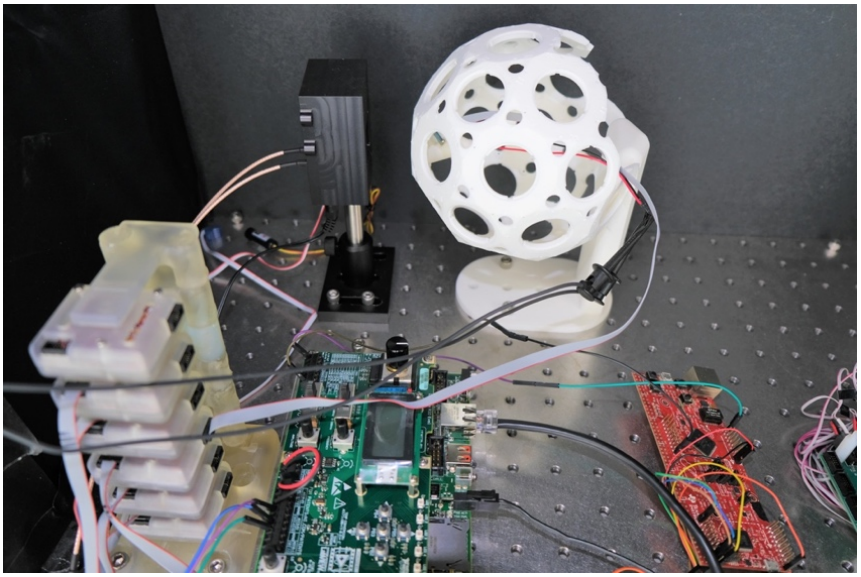

Figure 14. Test setup used for beam steering measurements.

A block diagram showing the various components used for the beam steering testing is presented in Figure 15. Steering commands are sent to the mirror via a microcontroller. The microcontroller relays these steering commands to the mirror driver board via a serial peripheral interface (SPI). A 16-bit LabView reconfigurable input/output (RIO) digitizer reads beam position information from the PSD. We record commanded and measured position for posterior processing.

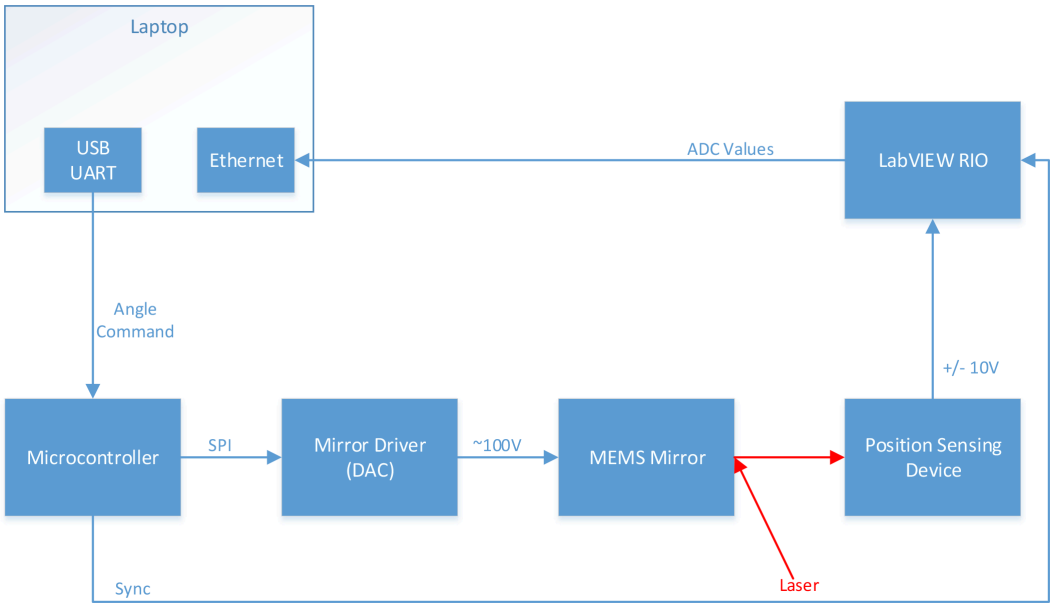

Figure 15. Block diagram showing the various components used during beam steering testing.

Figure 16 shows a plot of the measured steering angle as a function of the commanded angle. A polynomial function is used to generate the steering commands. Note that very good steering control is achieved. The RMS error obtained in these tests is 8 millidegrees.

We are continuing to upgrade our beam steering test setup, improve alignment, and minimize optical noise, in order to refine our steering measurements. Although the results obtained so far are encouraging, our goal is to achieve successful beam steering with RMS errors of a few millidegrees.

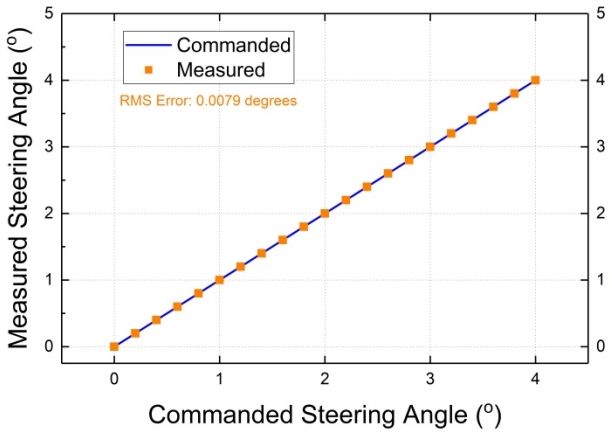

Figure 16. Plot of measured steering angle as a function of commanded angle.

C. Data Rate Testing

Data rate testing was performed using the setup shown in Figure 17. A modulatable laser mount was used as the optical source. The system optics were optimized to obtain a uniform optical spot on the detector. The receiver board includes an APD detector and a

transimpedance amplifier. A bit error tester (BERT) scope was employed to measure bit error rate (BER) and to observe signal quality via suitable eye diagrams. A calibrated power sensor was used to measure the power arriving to the detector.

With the current receiver board (which includes a 450 MHz TIA), we have been able to communicate at speeds of 600 Mbps. For this purpose, we programmed the BERTScope to generate a 600 Mbps pattern that was subsequently fed into the laser mount. The output of the TIA was connected back to the BERTScope.

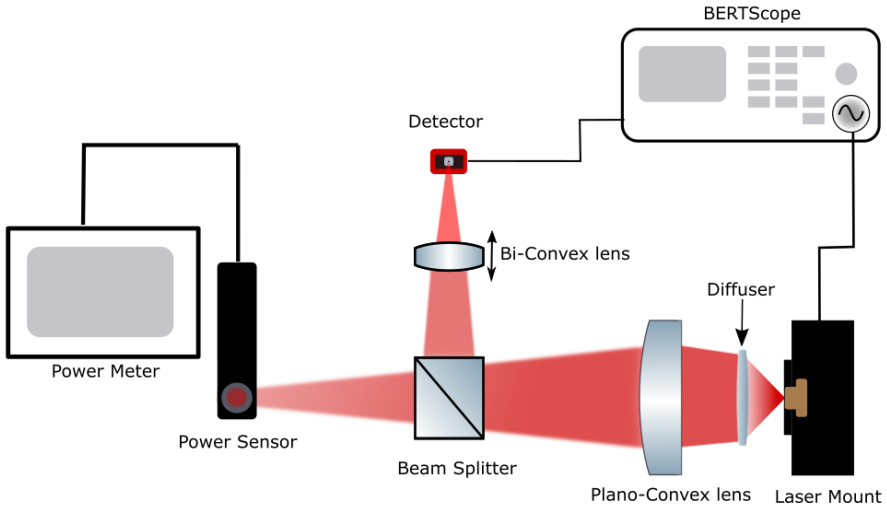

a)

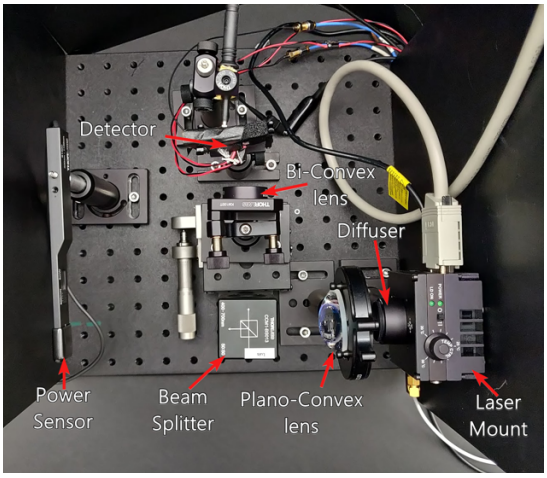

b)

Figure 17. (a) Schematic and (b) picture of the test setup employed for performing communications speed and sensitivity tests of the OOCN receiver.

Figure 18 shows an eye diagram obtained during this testing at 600 Mbps. Note that this diagram shows a very clear eye opening and relatively low jitter, which is indicative of proper operation of the receiver board at these high speeds. Also, the bit error rate measured during this test was 0 (ideal).

Our plans are to replace the TIA with a faster amplifier, which we have already identified, that can operate at above 1 Gbps. Once we perform this TIA upgrade, we believe we should be able to operate the OOCN at data rates of 1 Gbps and above.

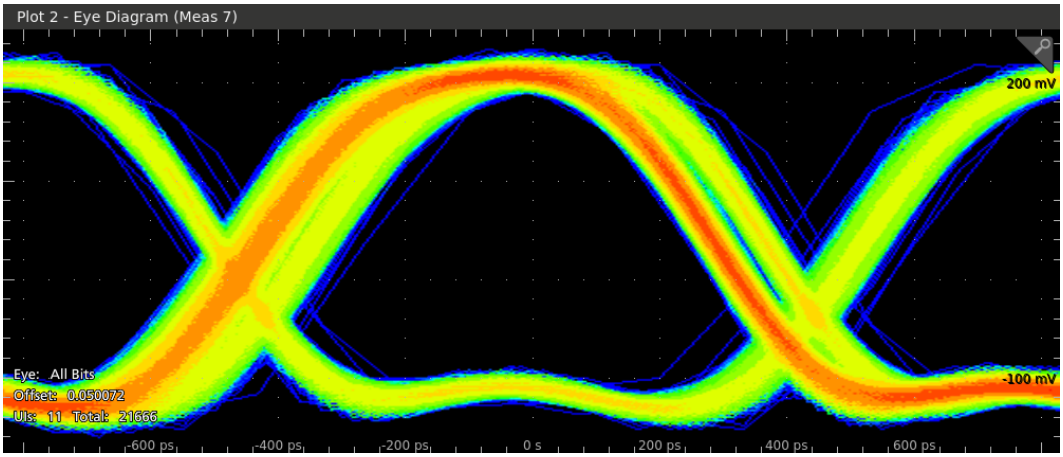

Figure 18. Eye diagram obtained with the setup shown in Figure 16 at 600 Mbps. The measured BER is 0.

D. Sensitivity

Receiver sensitivity is a key parameter for detecting optical signals at longer distances. We have performed sensitivity testing of our current receiver design using the setup shown in Figure 17.

For these tests, we use the BERTScope to generate a square wave and feed that signal into the laser mount. The TIA output was connected to the BERT for calculating bit error rates at various speeds. During these tests, we set the BERTScope at a given data rate and gradually began lowering the laser power, as we observed the TIA output on the BERT. We kept lowering the power until the measured BER fell below 10^{-6}. We performed these tests at speeds of 100 Mbps and 600 Mbps. At 100 Mbps, we obtained a received power of –63 dBm with a BER of 10^{-6}. At the faster speed of 600 Mbps, we obtained a BER of 10^{-6} at a received power of –52 dBm. All these tests are very encouraging indicators towards the high-speed capabilities of our OOCN receiver. We plan to perform further sensitivity testing once the new (faster) TIA amplifier is installed in our receiver.

V. Missions

As indicated earlier, we believe the OOCN could be a technology enabler for future swarm/constellation applications. In the case of closely arranged swarms, the OOCN should also be able to provide navigation metrology to determine the exact location of each spacecraft within the swarm. In this section, we provide a few examples of the type of future missions that could be facilitated by this new technology.

A. Q4

The Q4 mission is a technology demonstration low-earth-orbit (LEO) flight concept that is being proposed to show the advantageous capabilities of the OOCN [10]. The mission involves flying a swarm of four 6U CubeSats each furnished with OOCNs (Figure 19). The main purpose of the Q4 mission is to demonstrate: 1) full sky coverage, 2) gigabit-per-second data rates, and 3) ability to maintain multiple links simultaneously. The Q4 CubeSats are 6U spacecraft that will be furnished with proven high Technology Readiness

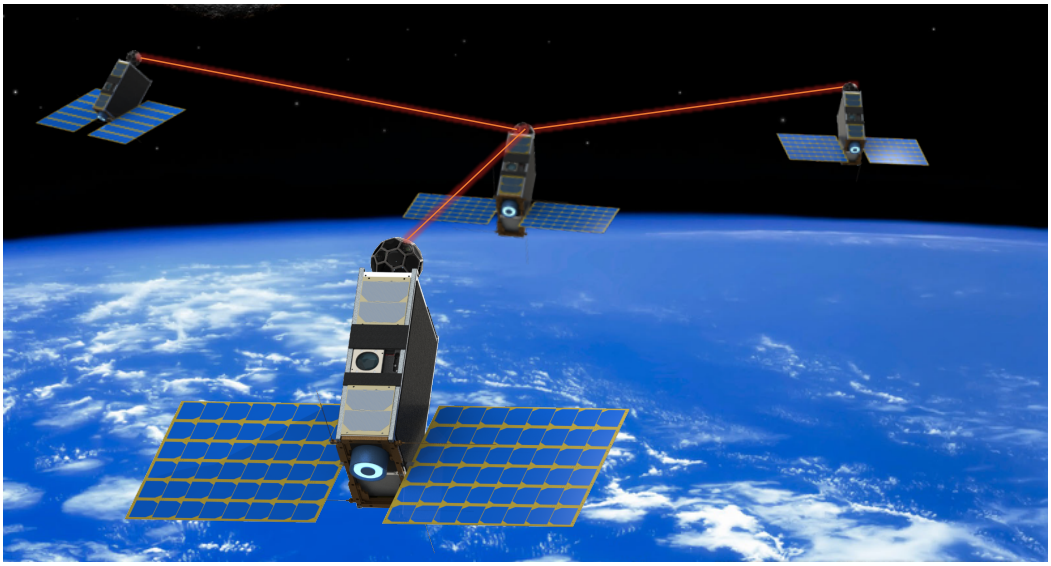

Figure 19. Proposed Q4 LEO mission to demonstrate the ISOC capabilities [10]. Q4 consists of four CubeSats: a leader and three followers.

Level (TRL) components for successful testing of the OOCN. We envision launching the four CubeSats as secondary payloads on a launch vehicle to the International Space Station (ISS) at an orbit altitude of 400 km, an inclination of 51.6°, and a right ascension of the ascending node (RAAN) of 257°.

The orbit being considered for the Q4 mission consists of one spacecraft in a circular orbit with a 400 km LEO altitude (referred to henceforth as the "leader"), and three other spacecraft ("followers") in slightly elliptical orbits surrounding the center spacecraft. The eccentricity of these other three orbits will cause the spacecraft to move relative to each other as they orbit the Earth, but all the orbits will have the same period, so that the relative motion is repetitive. The resulting azimuthal scan of the followers with respect to the leader will allow us to test and demonstrate the OOCN capabilities.

B. CADRE

This mission consists of a large number of small spacecraft furnished with high-frequency (HF) observation antennas to form a large aperture radio telescope for detecting HF emissions from exoplanets. The CubeSat Array for the Detection of RF Emissions from Exoplanets (CADRE) concept [11] involves the placement of a large swarm of CubeSats into small amplitude RF interference-free Lissajous orbits around the Earth–Moon L2 Lagrange point, as shown in Figure 20. In addition to the HF receivers, each CADRE CubeSat is to be furnished with JPL's OOCN, which should allow data sharing at gigabit per second data rates. Also, the relative azimuth and elevation between pairs of CubeSats should be established by the OOCN's AOA algorithm.

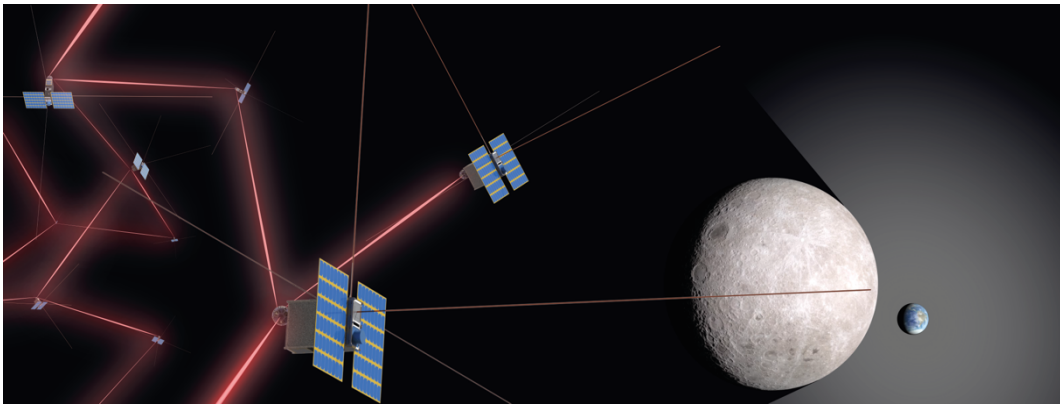

Figure 20. CADRE is a radio telescope concept located behind the moon that searches for potentially habitable exoplanets via their radio emissions [11]. The OOCN is a key enabling technology for this radio telescope.

C. Phase Array Radar

In Figure 21, we show a spaceborne phased array radar concept that could be implemented with a swarm of spacecraft. In this application, the leader is furnished with a HF radar transceiver and the followers with HF receivers. All the spacecraft are equipped with OOCNs. The beam width generated by a single HF antenna is typically large (>70°) and limits the spatial resolution of the radar target. This means that an HF spaceborne radar can only resolve the ground on swaths of several kilometers in diameter. If multiple spacecraft could be used to form a phased array radar, the resulting beam width could be greatly reduced by $1/n$ (where n is number of spacecraft). In typical operation, the leader would transmit the HF signal and each follower would receive the radar echoes from the target. The followers would then digitize and send, in real time, the echo information to the leader for subsequent processing of the image. The OOCN could provide not only connectivity to this radar swarm but also accurate navigation and position of each spacecraft, for accurate beam forming by the leader.

Figure 21. Spaceborne phase array radar enabled by the OOCN.

VI. Conclusions

We have presented JPL's new omnidirectional optical terminal that is being developed to provide fast connectivity and accurate metrology to swarms and constellations of spacecraft. We discussed the main features of the OOCN as well as its key capabilities. It was shown, based on preliminary experimental results, that the OOCN could accurately calculate the angle of arrival of incoming signals. It was also shown that the desired optical beam steering along the required field of regard could be attained with the current MEMS mirror. The OOCN can currently operate at rates of 600 Mbps but faster data rates are expected with ongoing upgrades to the receiver.

In addition, we discussed several missions that could be enabled by this technology. Q4 is a technology demonstration mission concept that includes four 6U CubeSats, each furnished with OOCNs, to demonstrate the novel capabilities of this revolutionary communications system. Future spaceborne radio telescope and phased array radar missions could also benefit from the OOCN's fast connectivity and accurate metrology. In general, the OOCN is ideally suited for crosslink communications among small spacecraft, especially for those forming a swarm and/or a constellation.

Acknowledgments

This work has been carried out with funding from NASA's Small Spacecraft Technology Program.

References

[1] D. M. Boroson, C. Chen, B. Edwards, "Overview of the Mars laser communications demonstration project," *2005 Digest of the LEOS Summer Topical Meetings,* July 25–27, 2005.

[2] D. M. Boroson, J. J. Scozzafava, D. V. Murphy, B. S. Robinson, "The Lunar Laser Communications Demonstration," *2009 Third IEEE International Conference on Space Mission Challenges for Information Technology,* July 19–23, 2009.

[3] D. J. Israel, B. L. Edwards, J. W. Staren, "Laser Communications Relay Demonstration (LCRD) update and the path towards optical relay operations," *2017 IEEE Aerospace Conference,* March 4–11, 2017.

[4] B. V. Oaida, M. J. Abrahamson, R. J. Witoff, J. N. Bowles Martinez, D. A. Zayas, "OPALS: An optical communications technology demonstration from the International Space Station," *2013 IEEE Aerospace Conference,* March 2–9, 2013.

[5] J. E. Velazco, "Omnidirectional Optical Communicator," in *IEEE Aerospace Conference Proceedings,* 2019, pp. 1–6.

[6] J. E. Velazco et al., "Inter-satellite omnidirectional optical communicator for remote sensing," *SPIE Opt. Eng. + Appl.,* vol. 10769, 2018.

[7] V. Milanović, et al., “Novel packaging approaches for increased robustness and overall performance of gimbal-less MEMS mirrors,” *Proc. SPIE 10116,* MOEMS and Miniaturized Systems XVI, 011607, February 20, 2017.

[8] G. Berkovic and E. Shafir, “Optical methods for distance and displacement measurements,” *Adv. Opt. Photon.,* vol. 4, no. 4, pp. 441–471, December 2012. http://aop.osa.org/abstract.cfm?URI=aop-4-4-441 .

[9] Space Chip Scale Atomic Clock, https://www.microsemi.com/product-directory/embedded-clocks-frequency-references/5207-space-csac .

[10] J.E. Velazco and J. Sanchez, “Q4 – a CubeSat Mission to Demonstrate Omnidirectional Optical Communications,” in *IEEE Aerospace Conference Proceedings,* 2020.

[11] M. de Kok, J. E. Velazco, and M. J. Bentum, “CubeSat Array for Detection of RF Emissions from Exoplanets using Inter-Satellites Optical Communicators,” in *IEEE Aerospace Conference Proceedings,* 2020.